Volume 32 | Number 8 | August 2017 | Pages 1437–1610

JAAS

Journal of Analytical Atomic Spectrometry

rsc.li/jaas

ISSN 0267-9477

ROYAL SOCIETY OF CHEMISTRY

PAPER

N. Hausmann *et al.*

Elemental mapping of Mg/Ca intensity ratios in marine mollusc shells using laser-induced breakdown spectroscopy

JAAS

PAPER

View Article Online
View Journal | View Issue

Cite this: J. Anal. At. Spectrom., 2017, 32, 1467

Elemental mapping of Mg/Ca intensity ratios in marine mollusc shells using laser-induced breakdown spectroscopy

N. Hausmann,[ab]* P. Siozos,[a] A. Lemonis,[a] A. C. Colonese,[b] H. K. Robson[b] and D. Anglos[ac]

Received 6th April 2017
Accepted 16th June 2017

DOI: 10.1039/c7ja00131b

rsc.li/jaas

Records of past environmental conditions in shell carbonate are usually derived from compositional analysis (*i.e.* trace elements, stable oxygen, carbon, and nitrogen isotopes) performed along the direction of the shell's growth and thus through time. However, compositional variations within isochronous parts of the shell can distort the environmental record and are difficult to assess without extensively mapping the whole shell. Here we apply Laser Induced Breakdown Spectroscopy (LIBS) to efficiently map the elemental change throughout the growth increments of three mollusc shells (*Conomurex fasciatus*, *Ostrea edulis*, *Anomalocardia flexuosa*). We employ an automated LIBS setup to map the Mg/Ca composition of whole shell sections with over 2000 data points per hour. By assessing the spatial variability of Mg/Ca intensity ratios this method has the potential to mitigate distorted results while increasing the resolution of derived palaeoenvironmental information.

Introduction

Carbonate from marine mollusc shells provides valuable records of past environmental conditions, such as salinity, sea surface temperature, and marine productivity. These records can be accessed by chemical analyses of shell carbonate (sclerochronology) based on stable isotope values ($\delta^{13}C$, $\delta^{15}N$, $\delta^{18}O$)[1,2] or the ratio of trace element concentrations (Mg/Ca, Sr/Ca, Li/Ca, Li/Mg, Sr/Li).[1] However, the correlation between environmental change and changes in the chemical composition can be highly variable and strongly dependent on the local environment as well as endogenous mechanisms.[3] These mechanisms are species specific or even specific to individual specimens of the same species.[4] In addition, elemental ratios can vary spatially even within isochronous parts of growth increments.[5–10] Such variations have been linked, for instance, to differences in the crystal fabric, such as distinct or gradual changes of crystal size, habit and orientation.[7] For example, in the case of *Arctica islandica* (Linnaeus, 1767) shells, Schöne *et al.*[8] suggest for best results, to restrict sampling to a single sublayer of the shell, which has favourable conditions of the crystal fabric and where Mg/Ca and Sr/Ca ratios are more consistent.

Studies of *Leukoma thaca* (Molina, 1782) link variations in isochronous parts to a zonation of Mg^{2+} transport in the outer epithelium of the mantle and into the extrapallial fluid, from which the shell is produced.[6] These variations were not consistent throughout the shell but they also varied between adult and juvenile parts. Zonation can also account for variations found in isochronous parts of *Pecten maximus* (Linnaeus, 1758) and *Mytilus edulis* (Linnaeus, 1758) shells.[6] In *P. maximus* only the mid and innermost parts are devoid of large variations, which is consistent for all analysed parts of the shell and does not seem to change as is the case for *L. thaca*.[7] However, Mg/Ca ratios in *M. edulis* are less defined by zonation and a strong influence of disturbance marks (distinct events linked to growth cessations) on the Mg/Ca ratio was found.[6] This is a general problem for sclerochronological analyses, as disturbance marks in *M. edulis* can be frequent and very irregular diachronically and between specimens.

A study of *Ruditapes philippinarum* (Adams & Reeve, 1850) by Poulain *et al.*[10] showed distinct differences in Mg/Ca ratios of the homogenous inner layer and the outer prismatic layer, as well as within parts of the outer prismatic layer. Despite constant growing conditions, the outside layer experienced an increase in Mg/Ca ratios through time, with the inside layer yielding lower values. Additionally, the Mg/Ca ratios within the outside layer decreased towards the exterior of the shell. However, this trend occurred inconsistently and was not present in all parts of the analysed section, effectively making this layer incapable of providing palaeoenvironmental data.

In a further study the isochronous layers within *Tridacna gigas* (Linnaeus, 1758) consistently produced different Mg/Ca

[a]Institute of Electronic Structure and Laser, Foundation for Research and Technology – Hellas (IESL-FORTH), P.O. Box 1385, GR 711 10 Heraklion, Crete, Greece. E-mail: niklas@palaeo.eu

[b]BioArCh, Department of Archaeology, University of York, UK

[c]Department of Chemistry, University of Crete, P.O. Box 2208, GR 710 03 Heraklion, Crete, Greece

ratios, with inner layers having higher Mg/Ca ratios than outer layers.[5] Additionally, a systematic bias related to shell age caused a general increase of Mg/Ca ratios and the seasonal amplitude in the inside layer of the shell only. This bias is still a matter of debate but is probably not linked to growth rates, given that the outer layer and the hinge part produced similar Mg/Ca ratios whilst having vastly different speeds of growth. The different baselines of Mg/Ca ratios in different layers allow for an indication of seasonal timing, which is useful in archaeological studies,[11] however difficult to interpret in terms of palaeotemperature.

In addition to the variation of Mg/Ca ratios between species, differences between specimens of the same species collected at different locations have also been identified.[3] Furthermore, variation has been encountered between specimens of the same species and locality.[4]

As the aforementioned studies demonstrate, mollusc shell chemistry and anomalies within shells are difficult to predict and no standard, reliable procedures exist that would to guide the sampling process and ensure an undistorted palaeoenvironmental record. In fact, a solution to avoid anomalies in the record for one specimen, would probably not be applicable in other specimens. As such, before the high resolution records of past environments can be interpreted with confidence, a screening process should be implemented in order to identify anomalous trends and spatial variations in the shell record.

It is common to assess Mg/Ca ratios and their spatial variation within shell carbonate by means of Laser Ablation-Inductively Coupled Plasma-Mass Spectrometry (LA-ICP-MS),[27] Inductively Coupled Plasma-Optical Emission Spectrometry (ICP-OES),[28] or microprobe techniques, which are highly accurate but time consuming. Thus, fast and more cost-effective methods of analysis can be of particular interest for this initial step of establishing environmental proxies.

In this context, Laser Induced Breakdown Spectroscopy (LIBS) is considered capable of addressing such problems in an effective manner. It features several distinct advantages such as high speed operation, minimal sample preparation, and *in situ* measurements.[29] The successful analysis of shell carbonate through LIBS has recently been reported[12–14] and the mapping in a pixel-by-pixel manner has been shown on various scales and materials including *in vitro* organic samples and geological settings.[15–18] However, the use of a time-efficient multi-elemental mapping feature to address elemental spatial variation in shell carbonate has not been explored as of yet.

In this study, we aimed to rapidly map Mg/Ca intensity ratios using LIBS and to identify compositional anomalies in isochronous growth increments of marine shells. We use two methods of data acquisition, a mapping method that displays spatial variations of elemental intensity ratios within the same growth increments, and a linear method that tracks changes in elemental composition along the growth direction of the shell. Using these methods, we analysed the shell of three marine species with a variety of mineral composition (aragonite, calcite), growth rate and growth pattern. The main goal of this study was to demonstrate firstly the feasibility of rapid automated and cost-effective sampling of marine records and secondly the potential of mapping spatial variations of environmental within shell structures.

Material and methods

Shell samples

Our study focused on modern and archaeological shells of three mollusc species, including the bivalves *Ostrea edulis* (Linnaeus, 1758) and *Anomalocardia flexuosa* (Linnaeus, 1767), and the gastropod *Conomurex fasciatus* (Born, 1778). The *Ostrea edulis* shell originated from the archaeological kitchen midden site of Krabbesholm, Denmark in 2000.[19] *Anomalocardia flexuosa* was collected in Laguna, Brazil, in 2009.[20] The shells of *Conomurex fasciatus* were sampled from the site JW1727 on the Farasan Islands, Saudi Arabia.[21] These species are economically relevant nowadays as well as in the past, and are widespread in archaeological and environmental deposits in the three regions.[19–21]

All three specimens had been previously used for stable isotope and sclerochronological analyses.[22,23] The shells had been previously prepared for sampling their microgrowth increments according to their form and shape. In the case of *O. edulis* a thin section (~18 μm) of the shell hinge was prepared; the *A. flexuosa* shell was sectioned along its growth axis and for *C. fasciatus* a thick section (~2 mm) was obtained from the last whorl of shell.

In all cases the shell samples were cut using a low-speed saw (Buehler, Isomet 1000) to expose the inner shell layers. *O. edulis* shells and *C. fasciatus* shells were embedded into a resin block (Buehler, EpoxyCure) to prevent breakage during the sectioning process. *A. flexuosa* shells only received a thin coating with epoxy resin (WIKO) prior to sectioning, which ensured protection of the cutting area. Subsequently, the sections were polished to provide a smooth surface and better visibility of the growth increments using successively finer metallographic grit papers (P800, P1200, P2500).

Experimental setup and calibration

In our experimental setup (Fig. 1), we employed a Q-switched Nd:YAG laser (Spectron Laser Systems), operating at the fundamental wavelength (1064 nm) and producing 10 ns pulses. The typical laser pulse energy used in this study was about

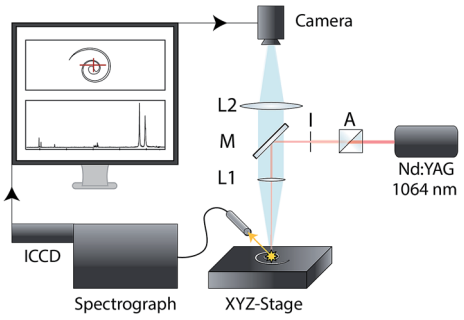

Fig. 1 Schematic diagram of the experimental setup. A: attenuator, I: iris, M: mirror, L1, 2: lenses.

10 mJ. The laser beam was focused on the sample using a quartz lens (L1) of 28 mm focal length. The focal point of the lens was set slightly below the sample surface and the working distance (focusing lens-to-sample distance) was adjusted so that a crater with a diameter of about 90 μm was measured on ablated spots performed directly on the sample. Thus, the laser irradiance was estimated to be approximately 16 GW cm^{-2}.

The shell sample was mounted on a motorized X–Y–Z micrometric translation stage (Standa Ltd.). For positioning the sample at the proper working distance, a black and white CCD camera (Point Grey Grasshopper 3) was placed in vertical alignment with the sample surface, the focusing lens (L1) and a dichroic mirror (M). By use of an additional lens (L2, $f = +120$ mm) a clear image of the sampling area was formed on the sensor of the camera (2736 × 2192 pixels) at a magnification of 4.2 : 1. This magnification is a compromise providing a general overview of the shell as well as good visibility of individual growth increments.

Measurements were performed at room temperature. The light emitted by the plasma plume was collected by an optical fiber of 200 μm core diameter and transmitted to a Czerny-Turner spectrograph (Jobin Yvon, TRIAX 320) for analysis in conjunction with an intensified charge coupled device (ICCD) detector (DH520-18F, Andor Technology). The spectrograph is equipped with a 600 grooves/mm grating providing a spectral resolution of about 0.1 nm. The ICCD is gated by means of a digital delay pulse generator (DG535, Stanford Research Systems) and synchronized to the Q-switch of the laser. Spectra were acquired at a delay time of $\tau_D = 500$ ns after the firing of the laser pulse with integration time of $\tau_G = 1$ μs. The entrance slit width of the spectrograph was set to 50 μm.

The selection of these acquisition parameters was based on a series of measurements performed under different delay and gate times, which revealed that for $\tau_D = 500$ ns and $\tau_G = 1$ μs both Mg and Ca emission lines had sufficient intensity and high S/N value, while continuum emission was negligible (Fig. 2A).

Several Ca and Mg emission lines were examined in the spectral range from 250 to 600 nm in order to identify those providing the most reliable Mg/Ca ratio. Three were the most essential requirements that had to be fulfilled by both Ca and Mg emission lines: (i) they had to be present within the 80 nm range of the spectrometer and adequately resolved with respect to adjacent emission lines, (ii) the intensity of the lines and particularly the Mg line had to be the highest available, in order to provide clean signals even at the lowest concentrations of Mg and (iii) they had to be generated from transitions of the same state of ionization (neutral or singly ionized atoms). The emission lines that fulfilled the above conditions were the Ca II ($^2D_{3/2} \rightarrow {}^2P_{1/2}$) emission line at 315.887 nm and the Mg II ($^2P_{3/2} \rightarrow {}^2S_{1/2}$) at 279.553 nm. Therefore, a spectral range centered around 300 nm was selected to record the LIBS spectra (Fig. 2A).

To verify the correlation between the Mg/Ca intensity ratio values measured and the Mg/Ca concentration ratio (mmol mol^{-1}) we followed the approach by Cobo *et al.*[12] using the same set of reference samples. These were composed of mixtures of magnesium and calcium carbonate powders, in different proportions (2–100 mmol mol^{-1}), incorporated into a silicone-rubber medium (Wacker Chemie AG, Elastosil M4601) having similar physical properties as the carbonate, found in marine shells, to account for matrix effects.[24] A very good positive linear relationship was obtained between Mg/Ca intensity ratios derived from the LIBS spectra and the Mg/Ca concentration ratios (Fig. 2B). Using the slope of the linear regression (b) and the standard deviation of the background (σ_B), we calculated a limit of detection (LoD)[24] on the order of 0.1 mmol mol^{-1} (100 ppm). Considering the significant intercept of the calibration curve, one could argue for an even lower LoD value. Commenting on this non-zero intercept, it is noted that literature reports show non-linear (saturating) calibration curves, obtained in LIBS measurements of magnesium in marble and soil samples, based on emission lines of Mg I (285.213 nm)[25] and Mg II (280.270 nm)[26] respectively. This saturation behaviour is most likely a result of self-absorption as both the Mg I and Mg II lines discussed are resonant ones. The non-linearity of the calibration curves reported[25,26] is quite evident for Mg concentration values starting in the low hundreds of ppm range and reaching over 2000 ppm, which approximately corresponds to the lowest Mg content reference sample used in the calibration curve shown in Fig. 2B.

Data acquisition

The dedicated software for the data acquisition process was developed using LabView 2015 (National Instruments) and was

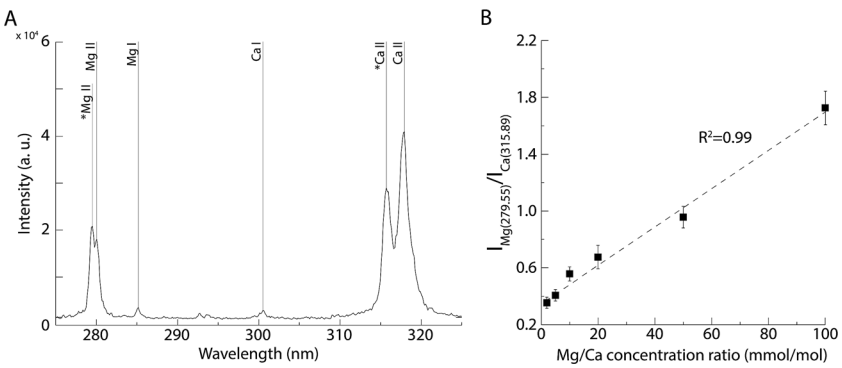

Fig. 2 (A): Single-shot LIBS spectrum of shell sample (measured peaks: Mg II: 279.553 nm and Ca II: 315.887 nm indicated by asterisks). (B): Calibration curve of Mg/Ca intensity ratio as a function of Mg/Ca concentration ratio.

divided into two phases. During the first phase, a sampling path was defined by moving the sample stage along a set of locations, which were targeted through the camera. Then, sampling points were interpolated along the path at a chosen interval (here 100 μm). The number of pulses and spectra per sample location could also be selected (here 10 pulses per spectra per sampling point). In the second phase, the motorised stage moved along the set of pre-selected sampling points, while acquiring LIBS spectra at each point. For each set of spectra, the mean intensity ratio of the two preselected wavelengths was calculated and allocated to the respective sample location.

Two modes of measurement could be chosen. The first mode was more suitable for quickly mapping elemental ratios, while the second mode was more suitable for detailed line-scans that follow the direction of shell growth and one-dimensionally track the elemental changes throughout the lifetime of the mollusc.

More specifically, the first mode (mapping) calculated the intensity ratio of selected peaks in an averaged spectrum derived from multiple (here 10) shots in the same sampling point.

The second mode (line scan) derived the average intensity ratio of selected peaks from a set of 10 single-shot spectra at each sampling point and calculates the corresponding standard deviation. The standard deviation provides a better assessment of fluctuations along the path of the line scan, but the processing of multiple single-shot spectra demands more time, thus it is omitted in the mapping mode.

The average time spent in a single sampling point was about 1.7 seconds in the mapping mode and 2.4 seconds in the line scan mode. These times are ultimately limited by the translation speed of the motorised stage, the distance between sample locations, the repetition rate of the laser, the pixel readout time of the CCD chip and the transfer time of the data from the ICCD camera to the computer. In our experiment, these limits must be added to the sequence of operations (including recording the spectrum, moving the sample to the next position, and waiting for the motor to stop) made by the software. These processes slow down the spectra acquisition rate to about 6 Hz and 4 Hz in the mapping mode and line scan mode, respectively. With this configuration a typical sampling path corresponding to 10 cm (=10 000 spectra) under the same experimental parameters (*e.g.* laser energy and working distance) required a total acquisition time of around 29 minutes (40 min in line scan mode).

Results

C. fasciatus

C. fasciatus shells have a conical structure, thus it is not possible to create flat sections that cover the entire shell record.[15] However, it is possible to access the most recent part of the record in the pronounced lip, which is formed during the adult stage when the shell growth rate decreases. The growth increments formed just prior to the adult stage are part of the same whorl and can also be accessed. In this specimen the last whorl is not entirely preserved and only 5 mm were available for analysis. A line scan was chosen that follows the curved direction of growth within the lip part of the shell. For this mode we chose a sample path (dashed line in Fig. 3A), which resulted in 68 sampling points. Mapping the entirety of the shell section resulted in a sampling path composed of 2356 sample locations. We found consistent Mg/Ca intensity ratios in both modes with values ranging between 0.04 and 0.11 in the line scan and 0.04 and 0.12 in the map (Fig. 3A and B).

The Mg/Ca intensity ratios in the line scan showed a clear oscillation along the lip, which likely reflects seasonal environmental changes. On the other hand, based on the mapping data the Mg/Ca intensity ratios exhibit local variations within the isochronous parts, which in some cases exceeded the overall variation observed throughout the growth increments. This was most obvious in the thinner part of the section prior to the lip, where two coeval layers of the shell grew in parallel but had consistently different Mg/Ca intensity ratios.

O. edulis

In their hinges, *O. edulis* shells provide very clear structures of their growth increments, which can be sectioned and sampled in straight lines to derive environmental temporal information.[16] This specimen of *O. edulis* provided a straightforward targeting process to investigate the elemental change through time, with a straight line scan of 54 sampling points. Mapping took place using 4298 sampling points. The results are shown in Fig. 3. Mg/Ca intensity ratios in both experiments were similar, albeit the mapped data reached similar minimum values (0.10 compared to 0.11) but higher maximum values (0.29 compared to 0.18). This is due to the mapping measurements sampling a wider area. Values for the same sample locations were almost identical.

Sequential samples in Fig. 3D showed a periodic change of the Mg/Ca intensity ratio that is repeated every 2–3 mm, with similar maxima and minima. This pattern is reflected in the mapped intensity ratios in Fig. 3C, although it is apparent that while the cyclical pattern persists, the minima and maxima changed within the same growth increments. Especially in the wider parts of the shell, at the end of the hinge (top right Fig. 3C), Mg/Ca intensity ratios are much higher than in the narrower parts (bottom left Fig. 3C). It is possible that the sampling area (90 μm) was too large to individually measure the maximum values in the narrower areas so the thinner growth increments carrying these values were mixed together with increments of lower values (time-averaging),[9] producing an average value that was lower than the actual maximum. In the wider parts, growth increments with maximum values are more likely to exceed the sampling resolution in thickness and can thus be sampled exclusively, resulting in a higher intensity ratio. However, the effect of time-averaging would equally affect growth increments carrying minimum values, which in this specimen is not the case as the minimum values of the wider parts of increments are also reached in narrower parts.

A. flexuosa

A sample path was chosen that follows the curved direction of growth, along which the 172 points were sampled. The mapping

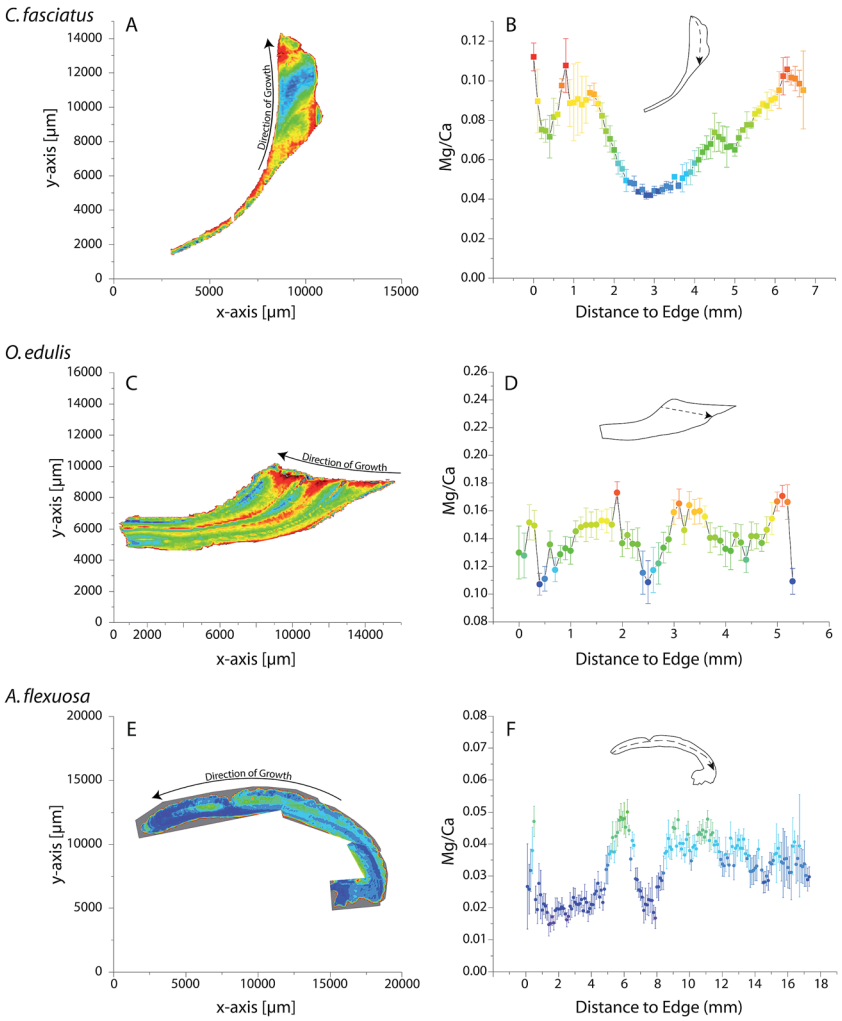

Fig. 3 LIBS analysis results (mapping and line scans) for the three shell sections. Direction of growth indicated by black arrow and sampling path for line scan is indicated on shell-outline as black dashed line. Colour mapping scale identical to corresponding line scan graph.

was carried out using 5888 sampling points. The Mg/Ca intensity ratios in *A. flexuosa* were again similar in both experiments, with the mapping experiment measuring higher maxima (0.12 compared to 0.05) and slightly lower minima (0.13 compared to 0.15). The gradual changes in the sequential values (Fig. 3F) are less regular than in the *O. edulis* shell but the individual cycles are consistent and present similar minima and maxima. The observed difference in cycle length is possibly due to changes in growth rate within the shell with a distinct period of slow growth between 6 and 9 mm distance to the shell edge. Additionally, there are signs of a complete growth stop at 0.3 mm distance to the shell edge. The abrupt decrease in Mg/Ca intensity ratio from 0.047 to 0.023 indicates that there has been a period of time that was not recorded in the shell.

The mapped values show large variations in Mg/Ca intensity ratios within isochronous parts (Fig. 3E). There is a general pattern where the central portion of growth increments produces higher Mg/Ca intensity ratios than parts of the same increment that are closer to the inside or outside edge of the shell. Similar 'zonation' was found in *Leukoma thaca*,[7] in *Mytilus edulis* as well as in *Pecten maximus*.[6] *A. flexuosa* shells consist entirely of aragonitic carbonate and no variations in mineralogy within them, which could explain the variations seen in the experiment, are known. Also, the entire outer layer of *A. flexuosa* shells is made of a crossed-lamellar structure.[20] Thus it provides no obvious structural reasons for the increase or decrease in intensity ratios. Despite this, it includes areas both high and low in Mg/Ca intensity ratios.

Conclusions

Here we demonstrate the application of an automated high-throughput LIBS setup capable of mapping Mg/Ca intensity ratios from shell carbonate *in situ*. This was realised with the use of a LIBS imaging system working with a spatial resolution at a scale of ~90 µm and an acquisition speed of ~20 000 spectra per h. Although regular and consistent changes in shell composition were visible, our study did not aim to link the elemental ratios to environmental change, but focused on the spatial variation of Mg/Ca intensity ratios that can potentially distort the environmental

signal or create artificial signals. Knowledge of this variation will greatly improve future studies that aim to assess the impact of environmental conditions on Mg/Ca variation as well as studies that aim to isolate biological processes that control elemental variations such as growth rate or zonation. Aspects of this study can also be extended to the measurement of additional elements (Sr, Ba, Li) important for environmental proxies. Thus, LIBS provides a cost-effective alternative for screening shell carbonate records in a fast and highly resolved way. Its application will be beneficial for carrying out more comprehensive studies of a variety of mollusc shells in different localities and environments.

Acknowledgements

We would like to thank Olga Kokkinaki for her valuable advice as well as Igor Gutiérrez-Zugasti, Adolfo Cobo and Asier García-Escárzaga for their helpful comments and for providing us with their reference samples. This research was funded by the EC, in the framework of a Marie Skłodowska-Curie Individual Fellowship to NH for the Project ACCELERATE ('Archaeological and climatic data from elemental ratios using rapid Analysis of shell carbonate'), Grant Agreement No. 703625. Preliminary work was supported in part through the transnational access activities of the EC FP7-Infrastructures-2011 project "Laserlab-Europe III", Grant Agreement No. 284464, Access project: ulf-forth-2012. ACC thanks São Paulo Research Foundation (FAPESP) project "Sambaquis e Paisagem" (Ref. 04/11038-0; Brazil) and the mobility grant (Ref. PA1002165) from the Spanish National Research Council (Spain) for sampling shells of Anomalocardia flexuosa. Permissions for sampling, exporting and analysing modern shells of Anomalocardia flexuosa were provided by ICMBio (IMABA, SISBIO; protocol no 113508). NH thanks the European Research Council for financing the sampling of C. fasciatus as part of the Advanced Grant DISPERSE (Ref. 269586).

References

1 B. R. Schöne and D. P. Gillikin, *Palaeogeogr., Palaeoclimatol., Palaeoecol.*, 2013, **373**, 1–5.
2 D. P. Gillikin, A. Lorrain, A. Jolivet, Z. Kelemen, L. Chauvaud and S. Bouillon, *Geochim. Cosmochim. Acta*, 2017, **200**, 55–66.
3 L. E. Graniero, D. Surge, D. P. Gillikin, I. Briz i Godino and M. Álvarez, *Palaeogeogr., Palaeoclimatol., Palaeoecol.*, 2017, **465**, 376–385.
4 J. E. Ferguson, G. M. Henderson, D. A. Fa, J. C. Finlayson and N. R. Charnley, *Earth Planet. Sci. Lett.*, 2011, **308**, 325–333.
5 M. Elliot, K. Welsh, C. Chilcott, M. McCulloch, J. Chappell and B. Ayling, *Palaeogeogr., Palaeoclimatol., Palaeoecol.*, 2009, **280**, 132–142.
6 P. S. Freitas, L. J. Clarke, H. Kennedy, C. A. Richardson and Others, *Biogeosciences Discussions*, 2009, **6**, 1209–1227.
7 C. E. Lazareth, F. Le Cornec, F. Candaudap and R. Freydier, *Palaeogeogr., Palaeoclimatol., Palaeoecol.*, 2013, **373**, 39–49.
8 B. R. Schöne, P. Radermacher, Z. Zhang and D. E. Jacob, *Palaeogeogr., Palaeoclimatol., Palaeoecol.*, 2013, **373**, 50–59.
9 K. Shirai, B. R. Schöne, T. Miyaji, P. Radermacher, R. A. Krause Jr and K. Tanabe, *Geochim. Cosmochim. Acta*, 2014, **126**, 307–320.
10 C. Poulain, D. P. Gillikin, J. Thébault, J. M. Munaron, M. Bohn, R. Robert, Y.-M. Paulet and A. Lorrain, *Chem. Geol.*, 2015, **396**, 42–50.
11 K. D. Thomas, *J. Archaeol. Sci.*, 2015, **56**, 159–167.
12 A. Cobo, A. García-Escárzaga, I. Gutiérrez-Zugasti, J. Setién, M. R. González-Morales and J. M. López-Higuera, *Appl. Spectrosc.*, 2017, DOI: 10.1177/0003702816687570.
13 A. García-Escárzaga, S. Moncayo, I. Gutiérrez-Zugasti, M. R. González-Morales, J. Martín-Chivelet and J. O. Cáceres, *J. Anal. At. Spectrom.*, 2015, **30**, 1913–1919.
14 Y. Lu, Y. Li, Y. Li, Y. Wang, S. Wang, Z. Bao and R. Zheng, *Spectrochim. Acta, Part B*, 2015, **110**, 63–69.
15 L. Sancey, V. Motto-Ros, B. Busser, S. Kotb, J. M. Benoit, A. Piednoir, F. Lux, O. Tillement, G. Panczer and J. Yu, *Sci. Rep.*, 2014, **4**, 6065.
16 H. Bette and R. Noll, *J. Phys. D: Appl. Phys.*, 2004, **37**, 1281.
17 Q. L. Ma, V. Motto-Ros, W. Q. Lei, M. Boueri, L. J. Zheng, H. P. Zeng, M. Bar-Matthews, A. Ayalon, G. Panczer and J. Yu, *Spectrochim. Acta, Part B*, 2010, **65**(8), 707–714.
18 T. Xu, J. Liu, Q. Shi, Y. He, G. Niu and Y. Duan, *Spectrochim. Acta, Part B*, 2016, **115**, 31–39.
19 H. Robson, PhD thesis, University of York, 2015.
20 A. C. Colonese, S. A. Netto, A. S. Francisco, P. DeBlasis, X. S. Villagran, R. Ponzoni, Y. Hancock, N. Hausmann, D. S. Faria, A. Prendergast and B. R. Schöne, *Palaeogeogr., Palaeoclimatol., Palaeoecol.*, 2017, DOI: 10.1016/j.palaeo.2017.01.006.
21 N. Hausmann and M. Meredith-Williams, *J. I. Coast. Archaeol.*, 2016, DOI: 10.1080/15564894.2016.1216478.
22 N. Hausmann, A. C. Colonese, A. de Lima Ponzoni, Y. Hancock, M. Meredith-Williams, M. J. Leng and G. N. Bailey, *Quaternary Int.*, 2015, **427**, 115–127.
23 N. Milner, *J. Archaeol. Sci.*, 2001, **28**(8), 861–873.
24 D. W. Hahn and N. Omenetto, *Appl. Spectrosc.*, 2012, **66**, 347–419.
25 V. Lazic, R. Fantoni, F. Colao, A. Santagata, A. Morone and V. Spizzichino, *J. Anal. At. Spectrom.*, 2004, **19**, 429–436.
26 B. Sallé, D. A. Cremers, S. Maurice and R. C. Wiens, *Spectrochim. Acta, Part B*, 2005, **60**, 479–490, DOI: 10.1016/j.sab.2005.02.009.
27 V. Mikko, W. G. Ambrose, P. E. Renaud, W. L. Locke, M. L. Carroll, J. Berge, L. J. Clarke, F. Cottier and H. Hop, *Palaeogeogr., Palaeoclimatol., Palaeoecol.*, 2017, **465**, 316–332; P. A. Tuan, W. Baeyens, M. Leermakers, S. Goderis, F. Vanhaecke and Y. Gao, *Talanta*, 2013, **115**, 6–14.
28 B. R. Schöne, Z. Zhang, D. Jacob, D. P. Gillikin, T. Tütken, D. G. -Schönberg, T. McConnaughey and A. Soldati, *Geochem. J.*, 2010, **44**(1), 23–37; S. Donna and K. C. Lohmann, *J. Geophys. Res.: Biogeosci.*, 2008, **113**(G2), G02001.
29 P. Westlake, P. Siozos, A. Philippidis, C. Apostolaki, B. Derham, A. Terlixi, V. Perdikatsis, R. Jones and D. Anglos, *Anal. Bioanal. Chem.*, 2012, **402**, 1413–1432; Z. E. Papliaka, A. Philippidis, P. Siozos, M. Vakondiou, K. Melessanaki and D. Anglos, *Heritage Sci.*, 2016, **4**, 15.

